NATO OTAN NURC
a NATO Research Centre
un Centre de Recherche de l'OTAN
NURC
PARTNERING FOR MARITIME INNOVATION

Reprint Series **NURC-PR-2012-003**

Volumetric reconstruction of oceanographic fields estimated from remote sensing and *in situ* observations from autonomous underwater vehicles of opportunity

Alberto Alvarez

April 2012

Originally published in:

IEEE Journal of Oceanic Engineering, Vol. 36, No. 1, January 2011, pp. 13-25.

About NURC

Our vision

- To conduct maritime research and develop products in support of NATO's maritime operational and transformational requirements.
- To be the first port of call for NATO's maritime research needs through our own expertise, particularly in the undersea domain, and that of our many partners in research and technology.

One of three research and technology organisations in NATO, NURC conducts maritime research in support of NATO's operational and transformation requirements. Reporting to the Supreme Allied Commander, Transformation and under the guidance of the NATO Conference of National Armaments Directors and the NATO Military Committee, our focus is on the undersea domain and on solutions to maritime security problems.

The Scientific Committee of National Representatives, membership of which is open to all NATO nations, provides scientific guidance to NURC and the Supreme Allied Commander Transformation.

NURC is funded through NATO common funds and respond explicitly to NATO's common requirements. Our plans and operations are extensively and regularly reviewed by outside bodies including peer review of the science and technology, independent national expert oversight, review of proposed deliverables by military user authorities, and independent business process certification.

NOTE: The NURC Reprint series reprints papers and articles published by NURC authors in the open literature as an effort to widely disseminate NURC products. Users are encouraged to cite the original article where possible.

Volumetric Reconstruction of Oceanographic Fields Estimated From Remote Sensing and *In Situ* Observations From Autonomous Underwater Vehicles of Opportunity

Alberto Alvarez

***Abstract*—A main challenge of military oceanography (MILOC) is to assess the oceanographic conditions of denied/high-risk marine regions. Monitoring technologies are limited to those that can provide access to these regions. Remote sensing and autonomous underwater vehicles (AUVs) can support MILOC requirements. Unfortunately, the environmental information gathered by these technologies is not complete: remote sensing provides information about some surface conditions and water-column integrated variables, whereas operational priorities often constrain AUVs use during real crisis situations to missions with higher priority than environmental assessment. Under this scenario, data fusion techniques to maximize the information of the collected data are essential. This paper attempts to reconstruct thermal fields fusing data gathered by remote sensing platforms and AUVs performing missions not specifically designed for environmental data collection. The technique estimates the state that maximizes the posterior probability subjected to some smoothing constraints. A variational methodology allows remote sensing information to serve as boundary constraints. The approach uses 3-D finite elements to solve the maximization problem. The procedure investigated has been tested with different smoothing constraints in a simulated environment and in a real field experiment conducted by the Muscle AUV in the Gulf of Riga (Baltic Sea) on April 19, 2008. Results highlight the relevance of incorporating the surface information provided by remote sensors into the estimation.**

***Index Terms*—Autonomous underwater vehicles (AUVs), finite elements, oceanographic sampling.**

I. Introduction

MILITARY OCEANOGRAPHY (MILOC) attempts to provide a timely meteorological and oceanographic (METOC) characterization of hostile littoral waters to which access is denied. Denied littoral waters are enemy held or disputed territorial waters, dangerously exposed waters adjacent to a severely threatened coastline, and regions not under the direct control of the enemy, but under his close surveillance. They introduce the classical asymmetry in the battlefield posed by the defender's advantage as holder of the battlespace over the attacker. Knowing the environment better than the adversary is a critical element to diminish the tactical asymmetry introduced by denied areas. Timely characterization of these regions is currently a challenging scientific and technological problem.

Until recently, *in situ* observational technologies fitting MILOC requirements of discretion and security were scarce. Environmental characterization of denied areas strongly depended on numerical approaches supported by remote sensing. Numerical ocean models of different spatio–temporal resolutions were nested in an attempt to downscale METOC information to the region of interest [34]. Complexity in the procedure and sensitivity to error propagation from large-scale simulations are the main drawbacks of this approach. Remote sensing is already recognized by the different navies as an important war-fighting tool [17]. Imaging radiometry, altimetry, and radar have been used to monitor hostile areas. Its application to coastal environments presents certain peculiarities that require higher spatial and temporal resolutions. Exploiting synergism with *in situ* measurements is of particular interest in this context.

Current technological capabilities can support a new methodology to characterize marine environments in hostile areas. This methodology relies on *in situ* observations rapidly carried out by coordinated fleets of autonomous robotic platforms, specially designed for real-time observation of the ocean environment, and complemented by remote sensing systems. Among these platforms are gliders, autonomous underwater vehicles (AUVs), and autonomous surface vehicles (ASVs).

AUVs represent a covert *in situ* capability to assess denied coastal areas [35]. These are submarine robots able to carry out expeditionary campaigns autonomously [11] whose hydrodynamic shape, electrical propulsion, and submarine navigation and positioning allow continuous sampling of environmental conditions. Their current main limitations are related to battery duration and the sophistication of submarine positioning and navigation. Military applications include mine hunting/neutralization and mine countermeasures (MCM); antisubmarine warfare (ASW) and ASW track and trail; intelligence, surveillance, and reconnaissance (ISR); target designation; and the collection of environmental data such as hydrographic/bathymetric surveys [36]. Among these applications, AUV capabilities for mine location and clearance operations are the most developed and employed, having been extensively tested during the real

Manuscript received October 15, 2009; revised May 24, 2010; accepted November 09, 2010. Date of publication January 28, 2011; date of current version March 18, 2011.

Associate Editor: H. Singh.

The author is with the NATO Undersea Research Center (NURC), La Spezia 19126, Italy (e-mail: alvarez@nurc.nato.int).

Color versions of one or more of the figures in this paper are available online at http://ieeexplore.ieee.org.

Digital Object Identifier 10.1109/JOE.2010.2092472

war scenarios such as the Operation Iraqi Freedom [21]. The technological maturity for this specific application and/or operational priorities have constrained the use of AUVs during real crisis situations to mine countermeasure operations in which autonomous vehicle follows preprogrammed tracks at a constant altitude from the bottom. Excursions to surface occur at sporadic assigned locations to validate or update the navigation system or to transmit data to the mother platform.

Conductivity–temperature–depth (CTD) sensors are standard in the suite of sensors carried by AUVs, and the data are collected by the vehicle while searching for mine-like objects. However, extracting environmental information from the CTD data gathered during mine countermeasure operations is difficult. This is because the trajectories followed by the AUV to search for mine-like objects do not constitute an optimal oceanographic sampling. Specifically, the volumetric space considered is not evenly sampled but measurements are dense on a hypersurface close to the bottom and in few vertical casts relatively distant from each other. In other words, locations of the given samples are very unequally distributed. Additionally, the high sampling rate of AUVs results in huge data sets, which are unusual in ship-based oceanography. These particularities prevent the use of geostatistical techniques commonly employed in oceanographic data analysis.

Traditionally, exploitation of oceanographic data requires representation of the sampled field on a regular grid which permits extracting dynamic information from the data. Estimation procedures are commonly employed to assign the best values at grid points on a regular grid from the data gathered at arbitrarily locations. One of the most commonly used estimation techniques is inverse distance weighted interpolation. These methods are also known as "Shepard methods" after the name of the first contributor in this field [37]. Shepard methods assumed that the interpolated values should be influenced more by nearby points and less by the more distant points. Specifically, the interpolated value at a target grid point is defined as a weighted sum of observed values. The weighting function is inversely proportional to the observation–gridpoint distance. All data points are used to estimate field values at unsampled locations. Distance-based schemes are in general less accurate and less efficient than other estimation approaches. Among their weaknesses, they tend to overweight data clusters. They also enforced radial isotropy around sample points, obscuring ridges and valleys in the field. Concerning their strengths, Shepard methods have the ability to extrapolate naturally outside the convex hull of the given data points. Finally, they are among most viable candidates for extension to three or more independent variables [4].

Radial basis function methods were initially proposed by [16] to interpolate scattered data from irregular surfaces. Interpolated values are obtained from a weighted sum of a family of nonlinear functions, called radial basis functions, centered at each observation. Multiquadratics, inverse multiquadratics, Gaussian, or Cauchy functions are commonly employed as radial basis functions. Weighting coefficients are obtained by enforcing the expansion to meet the observed values at sampled locations. While radial basis function methods are capable of very accurate fittings, they are not suitable for large data sets because they require a preprocessing stage of solving a system of linear equations that it dimensions with the number of data points. Application of radial basis function methods to oceanographic analysis is rather sparse in the literature [8].

Optimal interpolation schemes are of general use in oceanography [2], [29]. The approach relies on the locations where data are collected and an *a priori* knowledge of the covariance of the sampled field to provide the best linear estimation of the average and variance of the field at given unsampled locations. Specifically, the value of the field at an unobserved location is linked to a set of measurements using a discrete linear regression model. Regression coefficients are obtained from the variance and covariance relationship of the target field. If the spatial variability of the target field can be reasonably modeled as a Gaussian process, optimal interpolation is the best predictor (in terms of minimizing the mean square error), linear or nonlinear [33]. Optimal interpolation provides reliable estimates at locations inside the spatial extend spanned by the set of observations (properly known as interpolation problem) but problems may appear when estimating field values outside the convex hull defined by observations (extrapolation) [38]. Determination of a covariance model could be problematic in regions like coastal areas, where historical data may be sparse or nonexistent. Measured values, which are usually perturbed by errors, are met exactly in this approach causing frequently unacceptable errors in calculated derivatives. Similarly to radial basis function methods, optimal interpolation dimensions computationally with the number of samples and so is generally unfeasible for the very large data sets produced by AUV systems.

Volumetric estimations can be obtained complementing sparse *in situ* vertical profiles with remote sensing and historical data [28]. Briefly, this approach computes the empirical orthogonal function (EOF) decomposition of a multivariance matrix obtained from historical and present vertical profiles of different oceanographic variables. Temperature and sea height anomaly (SH) profiles are commonly employed to complement AUV observations of a target oceanographic field, because their surface values are easily obtained from remote sensing [sea surface temperature (SST) and sea surface height anomaly (SSH)] [30]. EOFs are defined by multicoupled modes, each containing patterns corresponding to the fields considered. Each field is then expanded in terms of a small number of corresponding modes of variability but with the same coefficients. Weighting coefficients are obtained by enforcing surface boundary conditions of the fields measured from satellite. Implementation of this multivariate procedure is limited by the existence of a dense historical data set in the region to build a representative multivariance matrix. Besides, determining SSH from altimetry in coastal areas is not always possible due to technical problems such as the land influence, the resolution of geophysical corrections, uncertainties of the mean sea level, and the low spatio–temporal resolution in regard to the coastal scales of variability [24].

Spline models are an alternative to previous estimation schemes [29], [42]. From a stochastic point of view, the technique provides the maximum-likelihood estimate from the data and *a priori* information that the first (membrane model) or

second derivatives (plate model) are zero everywhere and the result of random errors, i.e., white noise. In a more mathematical perspective, the approach is a regularization technique that stabilizes the inverse problem using a specific class of stabilizing functionals to restrict admissible solutions to spaces of smooth functions. Strengths of spline models are that they provide smooth estimations at unsampled locations, which are much better suited for derivative computations than previous procedures, they rely on *a priori* knowledge (smoothness of the field) of general applicability, and they dimension with the numerical grid used to solve the minimization problem. Their major drawback is that they do not characterize the uncertainty in the predictions. Spline techniques only provide the variance of the estimator. The lack of knowledge of a covariance function encoding the variability of the sampled field prevents the application of the Gauss–Markov theorem to compute prediction errors [9]. Spline models have been widely employed in different scientific disciplines like oceanography [6], [7], [29], geophysics [39], meteorology, and climatology among others [42].

A finite element formalism has been often employed to reconstruct continuous fields from experimental data using spline models in 2-D [5], [19] and 3-D [15]. The physical domain is divided in customary finite elements or cells in this approach. Continuous functions defined on this domain are approximated for each element in terms of some interpolation basis and function values at the element nodes. Similarly, function derivatives are computed from the derivatives of the interpolation basis and node values. Samples are represented in the same way. An advantage of this particular encoding is the substantial reduction of the dimensionality of the problem, being now dependent on the number of nodes of the finite element grid that discretizes the domain.

This paper investigates a procedure to estimate thermal conditions in a volumetric portion of a marine region from oceanographic data gathered by AUVs and remote sensors. AUV missions under consideration are not restricted to those designed to collect environmental data. The vehicles will be referred to as AUVs of opportunity in these cases. To the author's knowledge, this problem is addressed here for the first time. A variational approach with boundary constraints given by surface field data obtained through remote sensing is proposed to infer volumetric variability from sparse spatially biased data gathered by the AUV. Membrane and thin plate spline models are used to condition the resulting inverse problem, and their performance is compared. A finite element representation of the underlying oceanographic field is also suggested to numerically solve the system of equations resulting from the variational approach. The case of mine countermeasure operations is specifically treated here but the approach is easily generalized to any situation where AUV missions are not specifically designed for oceanographic sampling. The paper is organized as follows. Section II describes the mathematical aspects of the proposed methodology. Section III briefly summarizes the computational techniques applied to solve the problem. Application of the developed methodology is exemplified in Section IV. Finally, Section V discusses and concludes the work.

II. Mathematical Formalism

Let $\psi(x, y, z)$ be the generic scalar field we are interested to estimate in a given volume V of the ocean. Examples of ψ could be the temperature, salinity, or color fields. In principle, no *a priori* knowledge of the field is assumed except that it presents some coherence in space, that is, it does not change abruptly. This smoothness constraint is often expressed in terms of a probability that measures the extent to which the smoothness assumption is violated by a particular choice of $\psi(x, y, z)$. In 3-D continuous fields, smoothness terms often involve derivatives. Different orders of derivatives imply different smoothness. In particular, first

$$F(\psi) = \int\int\int_V |\nabla\psi|^2 dxdydz$$

or second

$$F(\psi) = \int\int\int_V \left|\nabla^2\psi\right|^2 dxdydz$$

derivative seminorms are commonly chosen as a smoothness constraint. These are known as membrane and thin plate models, respectively [25]. Membrane models assume *a priori* that the field has constant amplitude. A field with a constant spatial gradient is considered *a priori* if a thin plate model is used. In both cases, the *a priori* probability of the field follows a Gibbs distribution given by [22]

$$P(\psi) \propto e^{-(\alpha/2)F(\psi)} \tag{1}$$

with α being a scaling factor to be determined. The probability density (1) strongly penalizes those functional forms of ψ with high deviations from the *a priori* model in the volume V.

Let us suppose that the field has been sampled by an AUV following a path $(x(t), y(t), z(t))$, t being time, inside the volume V. The specific case of a single AUV is considered here; application of the method can be extrapolated when more AUVs are present. No restrictions are imposed on the trajectory. The output of the sampling process is a set of measurements taken at discrete locations $d = \{d(x_i, y_i, z_i)\}_{i=1\ldots N}$, where the number of samples N could be very large (up to tens of thousands). It is assumed that the observation of the AUV at a given location (x_i, y_i, z_i) is the true value of the field at this location $\psi(x_i, y_i, z_i)$ plus an independent Gaussian noise $\varepsilon(x_i, y_i, z_i)$ characterized by a standard deviation $\sigma(x_i, y_i, z_i)$. Under this assumption, the probability to get the set of measurements $\{d(x_i, y_i, z_i)\}_{i=1\ldots N}$ for a given realization of the field $\psi(x, y, z)$ is provided by the likelihood density [39]

$$p(d\,|\psi\,) \propto e^{-\sum_{i=1}^{N}\left((\psi_i - d_i)^2/2\sigma_i^2\right)}. \tag{2}$$

According to Bayes' rule, the posterior probability of having the field $\psi(x, y, z)$ given the set of observations $\{d(x_i, y_i, z_i)\}_{i=1\ldots N}$ is

$$P\,(\psi\,|d\,) = \frac{p\,(d\,|\psi\,)\,P(\psi)}{p(d)} \tag{3}$$

where $p(d)$ is the probability density of the observations, which is constant when d is given. Substitution of (1) and (2) in (3) gives [39]

$$P(\psi\,|d) \propto e^{-\sum_{i=1}^{N}\left((\psi_i-d_i)^2/2\sigma_i^2-(\alpha/2)F(\psi)\right)}. \quad (4)$$

The maximum *a posteriori* (MAP) estimate is defined by the field $\psi^{\mathrm{MAP}}(x,y,z)$ that satisfies

$$\psi^{\mathrm{MAP}} = \arg\min_{\psi}\left(\sum_{i=1}^{N}\frac{(\psi_i-d_i)^2}{2\sigma_i^2}+\frac{\alpha}{2}F(\psi)\right). \quad (5)$$

$\psi^{\mathrm{MAP}}(x,y,z)$ is then the most probable field compatible with our level of knowledge described by the smoothness constraint and the data collected by the AUV.

The field $\psi^{\mathrm{MAP}}(x,y,z)$ can be calculated using a variational approach. Variational principles have been widely used in meteorology [1], [10], [18], [23] and oceanography [14], [27]. The selection of a variational procedure to solve (5) is adopted here because variational calculus includes boundary conditions in an elegant fashion [12]. This feature facilitates later the integration of remotely sensed data into the formalism. After some manipulation, condition (5) can be written as (6), shown at the bottom of the page, for the membrane model and (7), shown at the bottom of the page, for the thin plate model. In both equations, S is the surface enclosing the volume V and $\delta(x,y,z)$ is the 3-D Dirac delta. Because variations of the field $\delta\psi$ are independent, relation (6) holds if the field satisfies the associated Euler–Lagrange differential equation

$$\sum_{i=1}^{N}\frac{\left(\psi_i^{\mathrm{MAP}}-d_i\right)}{\sigma_i^2}+\alpha\nabla^2\psi^{\mathrm{MAP}}=0 \quad (8)$$

with the natural boundary condition $\nabla\psi^{\mathrm{MAP}}\,|_S\,\hat{n}=0$ or Dirichlet boundary condition $\delta\psi^{\mathrm{MAP}}\,|_S=0$. Similarly, (7) derives the Euler–Lagrange equation

$$\sum_{i=1}^{N}\frac{\left(\psi_i^{\mathrm{MAP}}-d_i\right)}{\sigma_i^2}+\alpha\nabla^4\psi^{\mathrm{MAP}}=0 \quad (9)$$

subjected to Dirichlet boundary conditions $\delta\psi^{\mathrm{MAP}}\,|_S=0$ or natural boundary conditions $\nabla\left(\nabla^2\psi^{\mathrm{MAP}}\right)|_S\,\hat{n}=0$ and $\nabla^2\psi^{\mathrm{MAP}}\,|_S=0$. In this study, satellite data will be incorporated to impose a Dirichlet boundary condition at the sea surface while natural boundary conditions are assumed in the rest of the boundary surfaces where no information is available.

Summarizing, the estimation of the field $\psi(x,y,z)$ in the volume V is the maximum of a posterior solution of a probability that takes into account the assumption of smoothness of the field and the data obtained from the AUV and remote sensors. *In situ* data gathered from the AUV are source terms of the Euler–Lagrange equation derived from the optimization process, while satellite data constrain the boundary values at one of the boundary surfaces of the domain. This procedure optimizes the exploitation of information available from remote sensors and AUVs.

III. Computational Method

A 3-D finite element approach has been programmed to solve the mathematical problem described in Section II. The total volume V under consideration is discretized with an unstructured mesh constituted by elementary volume units. The unstructured character of the mesh allows easy adaptation to the irregularities of the boundaries showing finer resolution in very irregular regions. Different geometries of the volume element can be considered to build the mesh. The geometry of a triangle-based prismatic element is considered in this work. This geometry provides enough accuracy to solve the proposed mathematical problem while maintaining reasonable computational requirements [13]. The prismatic element is defined by 15 nodes (Fig. 1). This is the simplest prismatic element that supports computation of second derivatives of the field.

The finite element procedure encodes the value of any function $\psi(x,y,z)$ inside the prismatic element by the value of the function at each node and a set of interpolation functions

$$\psi(x,y,z)=\sum_{i=1}^{15}N_i(r,s,t)\psi_i \quad (10)$$

$$\begin{aligned}
&\iiint_V\left(\sum_{i=1}^{N}\frac{\left(\psi^{\mathrm{MAP}}-d_i\right)}{\sigma_i^2}\delta\left(x_i,y_i,z_i\right)\delta\psi+\alpha\nabla\psi^{\mathrm{MAP}}\nabla\delta\psi\right)dxdydz\\
&=\iiint_V\left(\sum_{i=1}^{N}\frac{\left(\psi^{\mathrm{MAP}}-d_i\right)}{\sigma_i^2}\delta\left(x_i,y_i,z_i\right)-\alpha\nabla^2\psi^{\mathrm{MAP}}\right)\delta\psi\;dxdydz+\oiint_S\alpha\left(\nabla\psi^{\mathrm{MAP}}\hat{n}\right)\delta\psi\;dS\\
&=0
\end{aligned} \quad (6)$$

$$\begin{aligned}
&\iiint_V\left(\sum_{i=1}^{N}\frac{\left(\psi^{\mathrm{MAP}}-d_i\right)}{\sigma_i^2}\delta\left(x_i,y_i,z_i\right)\delta\psi+\alpha\nabla^2\psi^{\mathrm{MAP}}\nabla^2\delta\psi\right)dxdydz\\
&=\iiint_V\left(\sum_{i=1}^{N}\frac{\left(\psi^{\mathrm{MAP}}-d_i\right)}{\sigma_i^2}\delta\left(x_i,y_i,z_i\right)+\alpha\nabla^4\psi^{\mathrm{MAP}}\right)\delta\psi\;dxdydz+\oiint_S\alpha\left(\nabla^2\left(\psi^{\mathrm{MAP}}\right)\nabla\delta\psi-\nabla\left(\nabla^2\psi^{\mathrm{MAP}}\right)\delta\psi\right)\hat{n}\;dS\\
&=0
\end{aligned} \quad (7)$$

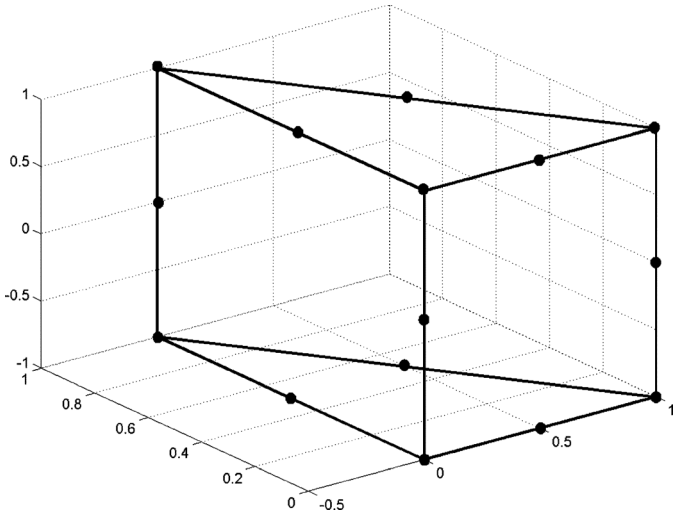

Fig. 1. Prismatic element with 15 nodes.

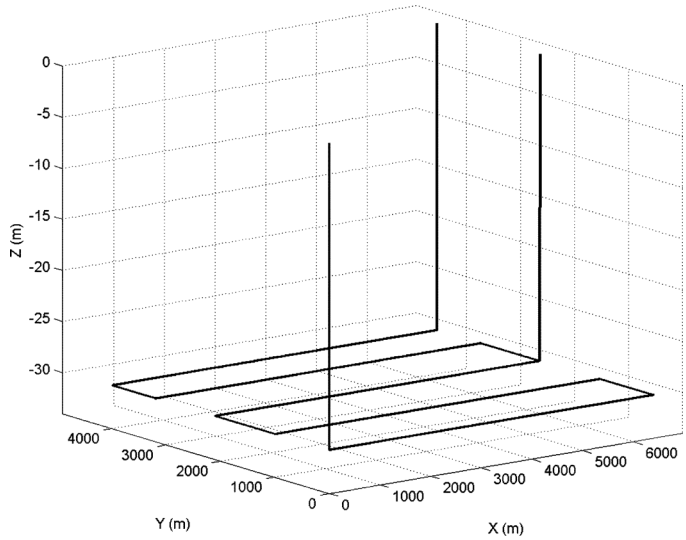

Fig. 2. Trajectory simulating a mine countermeasure mission for an AUV.

where ψ_i is the value of the function at node i and $N_i(r,s,t)$ represents the interpolation functions expressed in a local coordinate system $\{r,s,t\}$ [13]. The specific mathematical expressions of these functions are not replicated here as they can be easily found in different textbooks about finite elements [13], [41]. An advantage of this encoding is that the computational demand depends on the total number of nodes considered in the mesh and not on the size of the data set. This permits to process huge amount of data with limited computational effort. To provide an idea, data sets up to 3.7×10^4 samples have been processed in this work using the described finite element approach.

Substitution of (10) into (6) and (7) results in a system of linear equations for the unknown values of the field at the nodes

$$\left({K^M}_{ij} + A_{ij}\right)\psi_j = g_i \tag{11}$$

$$\left({K^{TP}}_{ij} + A_{ij}\right)\psi_j = g_i \tag{12}$$

for the membrane and thin plate models, respectively. Matrices are given by (13), shown at the bottom of the page, where V_e and N_e are the volume and data inside a prismatic element and superscripts M and TP refers to membrane and thin plate models, respectively. Systems (11) and (12) are solved, after adequately introducing the boundary conditions, to obtain the values of the field at the nodes of the mesh.

The method described is of little practical use unless the smoothing parameter α can also be estimated. Previous oceanographic studies made use of heuristic considerations to determine the value of α [6], [7]. A more objective assessment of the smoothing parameter is obtained using the generalized cross-validation (GCV) procedure [42]. GCV is a predictive mean square error criterion that has been widely employed in other scientific disciplines, including numerical weather prediction [43], image processing [3], astronomy [40], and chemistry [20]. For the present case, the GCV estimate of α in (11) and (12) is the minimizer of $V(\alpha)$

$$V(\alpha) = \frac{\frac{1}{N}\|I - H(\alpha)g\|^2}{\left(\frac{1}{N}\mathrm{Trace}\left(I - H\left(\alpha\right)\right)\right)^2} \tag{14}$$

with N being the total number of nodes, I the identity matrix, and H the influence matrix defined by

$$H\left(\alpha\right) = A\left(A^TA + \alpha^2{K^{M(TP)}}^T K^{M(TP)}\right)^{-1}A^T \tag{15}$$

with superscript T standing for transpose operation. The minimization is suggested to be done over the interval $(0, \sqrt{\mu_A/\mu_K}]$

$$\begin{aligned}
{K^M}_{ij} &= \alpha\int\int_{V_e}\int\left(\frac{\partial N_i}{\partial x}\frac{\partial N_j}{\partial x} + \frac{\partial N_i}{\partial y}\frac{\partial N_j}{\partial y} + \frac{\partial N_i}{\partial z}\frac{\partial N_j}{\partial z}\right)dxdydz\\
{K^{TP}}_{ij} &= \alpha\int\int_{V_e}\int\left(\frac{\partial^2 N_i}{\partial x^2}\frac{\partial^2 N_j}{\partial x^2} + \frac{\partial^2 N_i}{\partial y^2}\frac{\partial^2 N_j}{\partial y^2} + \frac{\partial^2 N_i}{\partial z^2}\frac{\partial^2 N_j}{\partial z^2} + 2\frac{\partial N_i}{\partial x}\frac{\partial N_j}{\partial y} + 2\frac{\partial N_i}{\partial x}\frac{\partial N_j}{\partial z} + 2\frac{\partial N_i}{\partial y}\frac{\partial N_j}{\partial z}\right)dxdydz\\
A_{ij} &= \sum_{k=1}^{N_e}\frac{N_i\left(\vec{x}_k\right)N_j\left(\vec{x}_k\right)}{\sigma_k^2}\\
g_i &= \sum_{k=1}^{N_e}\frac{N_i\left(\vec{x}_k\right)d\left(\vec{x}_k\right)}{\sigma_k^2}
\end{aligned} \tag{13}$$

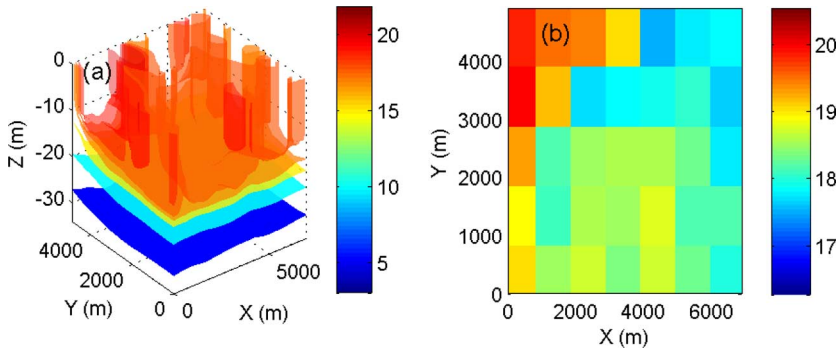

Fig. 3. (a) Simulated 3-D temperature field and (b) corresponding coarse grained surface conditions emulating satellite measurements. Colorbar units: degrees Celsius.

with μ_A and μ_K being the largest magnitude eigenvalues of $A^T A$ and $K^{M(TP)^T} K^{M(TP)}$, respectively.

IV. Results

A. Simulated Environment

The mathematical and computational methodologies described in Section III have been tested in a virtual environment. An arbitrary marine region of 7×5 km^2 is considered (Fig. 2). The area is 35 m deep, which is representative of many mine countermeasure operations. A mine countermeasure operation is programmed for a virtual AUV. The mission consists of tracing five legs of 7-km length with a spacing of 1 km apart from each other. The vehicle navigates at an altitude of 5 m from the bottom. Three vertical trajectories in the water column are assumed corresponding to depth excursions of the vehicle.

During its flight, the AUV is assumed to cross through water masses of different thermal signature. Fig. 3(a) shows the complexity of the 3-D structure of the temperature field considered. This field is characterized by strong temperature gradients, ranging from water masses of 5 °C near the bottom to more than 20 °C at some surface locations. Isothermal tubular structures going from surface up to 20-m depth populate the warmest area. These structures would resemble those generated by turbulent mixing. A thermograph of the sea surface temperature is simulated by coarse representation of the surface layer of the 3-D temperature field. Resolution of the thermograph data is 1 km, emulating the typical resolution of the advanced very high resolution radiometer (AVHRR) sensors [Fig. 3(b)]. The simulated data set gathered by the AUV is constituted by 36 093 samples, corresponding to a sampling frequency of a measurement per meter of trajectory (1 Hz at 2 kn). The degree of environmental complexity generated to test the developed procedures is not very likely to occur in the real ocean, except perhaps in extreme estuarine conditions involving river outflows of very cold water into a very warm sea. However, it provides an excellent framework to test the algorithms.

A 3-D grid of 1532 nodes and 462 prismatic elements was generated in the region of interest (Fig. 4). This grid corresponds to segmenting the volume with seven layers of prismatic elements of 5-m depth and triangular faces with approximate 1-km edges. Fig. 5(a)–(d) shows the temperature field estimated from the AUV data using the membrane and thin plate models

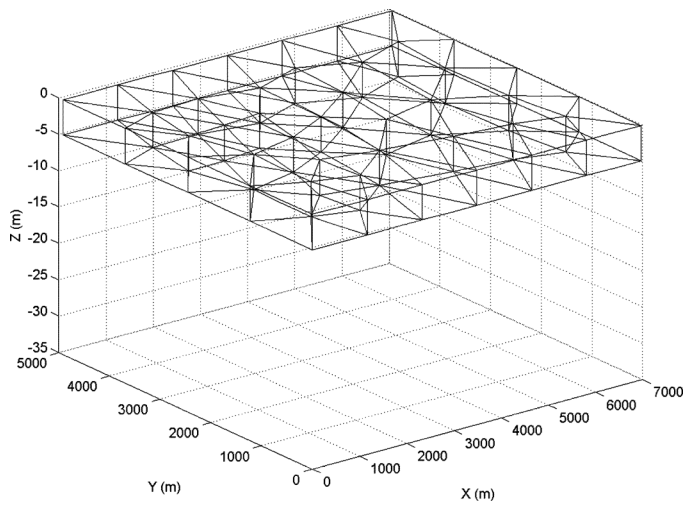

Fig. 4. First layer of prismatic elements.

with and without incorporating satellite information. Similarly to Fig. 3(a), isothermals corresponding to 20 °C, 19 °C, 18 °C, 17 °C, 15 °C, 10 °C, and 5 °C are displayed in Fig. 5(a)–(d). A membrane model without satellite information generates a vertically layered thermal field [Fig. 5(a)]. Information from the variability of the most superficial layers is only captured at the first vertical trajectory, but rapidly smooths out in the volume. A substantial modification in the estimated field is obtained with the incorporation of satellite information to the membrane model [Fig. 5(b)]. A higher spatial variability is now observed at the surface layers. A doming of the isothermal of 18 °C is found at the rightmost corner of the domain. This region is characterized by a high spatial variability described by a number of small-scale tubular structures. Satellite resolution is not high enough to resolve these small structures, resulting in a rather homogeneous surface region with temperatures close to 18 °C. The warm structure existing in the leftmost corner of the domain is partially recovered. Finally, notice that the surface doming is also extrapolated to the isothermal of 5 °C. Fig. 5(c) displays the estimations obtained by the thin plate model without including satellite information. Direct comparison with Fig. 5(a) reveals a bigger impact from the data gathered in the vertical trajectories of the AUV. Finally, Fig. 5(d) displays the isothermals

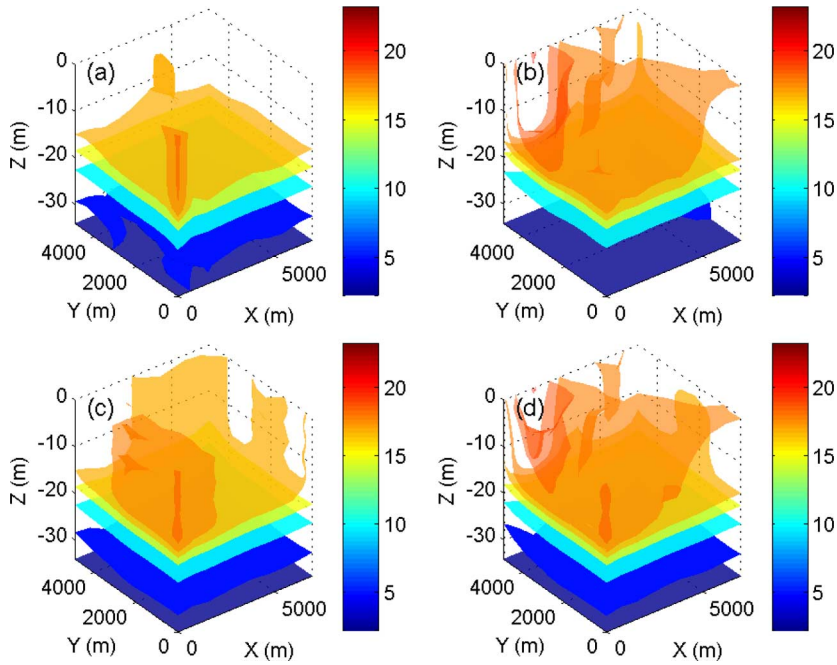

Fig. 5. Estimations of the temperature field obtained with (a) the membrane model without satellite information, (b) the membrane model with satellite information, (c) the thin plate model without satellite information, and (d) the thin plate model with satellite information. Colorbar units: degrees Celsius.

estimated with the thin plate model incorporating satellite information. Estimated surface variability increases. Similarly to the membrane model, a doming of the 18 °C isothermal is predicted. However, the warm structure of the leftmost corner of the domain is better defined than in the previous case. Finally, the estimated isothermal of 5 °C is a surface parallel to the bottom as in the original data.

A more quantitative evaluation of the performance of the different model is obtained from a scatter plot representing the estimated versus real temperatures at the nodes of the grid (Fig. 6). Fig. 6(a) confirms the layered nature of the field estimated with the membrane model without satellite information. The computed estimation error is 0.99 °C. Similar estimation error is found for the case of the membrane model incorporating satellite information [Fig. 6(b)]. A substantial part of this error is attributed to the wrong estimation obtained for the deepest isothermals. Remarkable deviations are found at spatial locations with temperatures lower than 5 °C. Fig. 6(c) and (d) shows substantial improvements in the estimated field when the thin plate model is used. Estimation errors are 0.72 °C and 0.56 °C for estimations without and with satellite information, respectively. Fig. 7(a)–(d) displays the 3-D distribution of the estimation error, providing additional intuition to the analysis. Comparison of Fig. 7(a)–(d) shows the impact of satellite data on estimations. Significant deviations from true temperature values are found in the membrane model without satellite information, out of the AUV horizontal sampling plane and vertical casts [Fig. 7(a)]. The approach underestimates the temperature except in the deepest layer, showing a positive error gradient with depth. Inclusion of satellite data partially corrects the deficiency found in the previous estimations [Fig. 7(b)]. The estimation error diminishes in the first 20 m of the water column. Notice that the correction seems to be done through

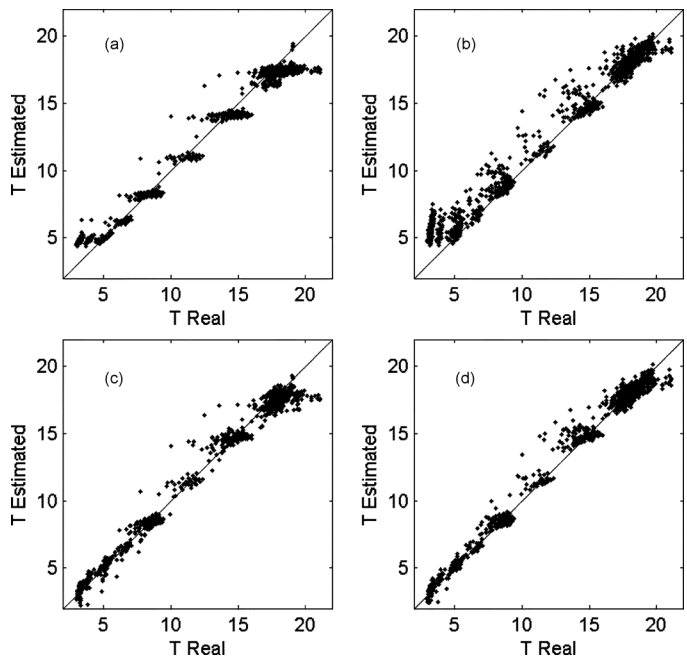

Fig. 6. Comparison of real versus estimated temperatures obtained from (a) the membrane model without satellite data, (b) the membrane model with satellite data, (c) the thin plate model without satellite data, and (d) the thin plate model with satellite data.

adding a temperature offset that warms up the whole water column, resulting in relevant positive errors in areas distant from vertical casts (leftmost corner of the volume). Concerning the thin plate model, Fig. 7(c) and (d) reinforces the benefits of adding satellite information to the estimation process. Finally, comparison of Fig. 7(a)–(d) confirms the superior performance of the thin plate model when compared to the membrane model.

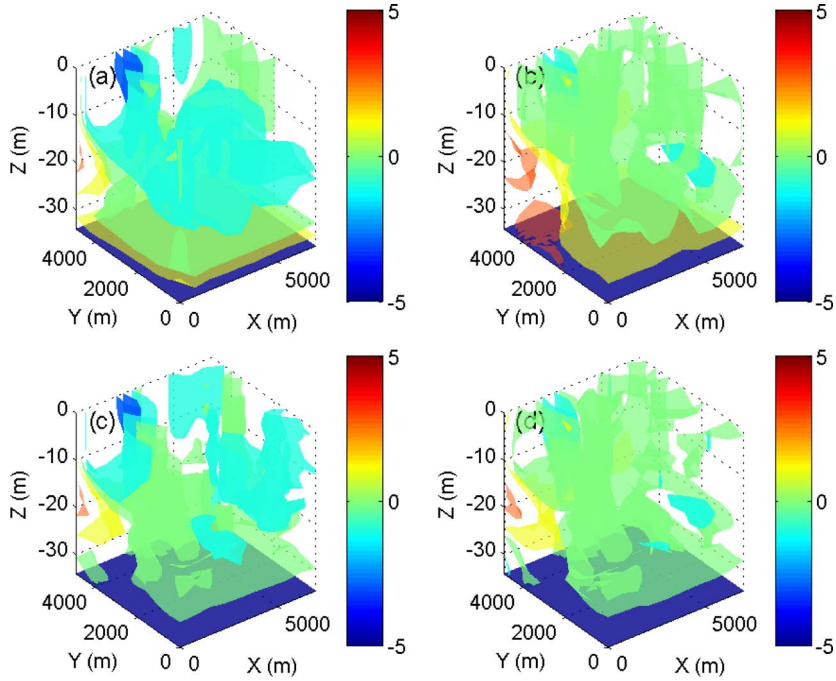

Fig. 7. Errors in the temperatures estimated from (a) the membrane model without satellite data, (b) the membrane model with satellite data, (c) the thin plate model without satellite data, and (d) the thin plate model with satellite data. Colorbar units: degrees Celsius.

Fig. 8. Muscle AUV employed during *Colossus 2* experiment.

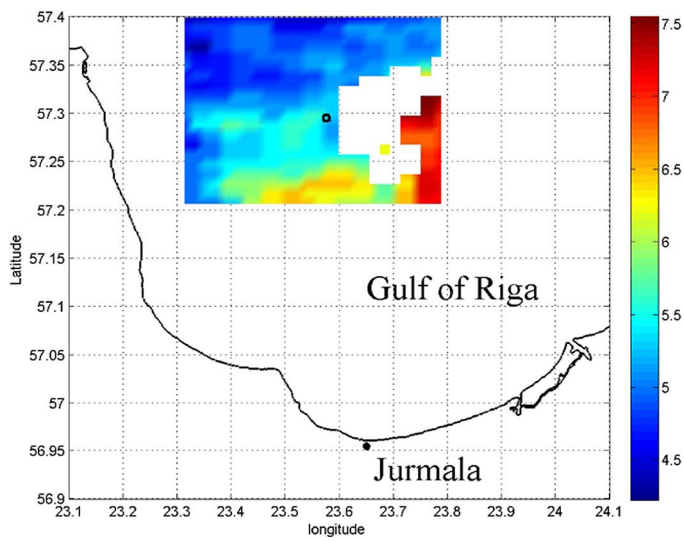

Fig. 9. Area of operations and AVHRR-SST in the Gulf of Riga corresponding to April 19, 2008. Colorbar units: degrees Celsius.

B. Field Experiment

A field experiment named *Colossus-2* was conducted by the *NR/V Alliance* from the NATO Undersea Research Center (NURC, La Spezia, Italy) during April 2008 at different locations off the coast of Latvia. The main scope of the cruise was to search for objects of interest (OOI), surveying the sea bottom with the Muscle AUV (Fig. 8). Muscle is 3.5 m in length, has a diameter of 0.52 m, weights 500 kg, and develops a nominal speed of 1.6 ms^{-1}. This AUV is equipped with a synthetic aperture sonar (SAS) operating at frequencies of around 300 kHz to perform large-area search and survey of the sea bottom. A CTD-ER-1-0-700-200 from RD Instruments (Poway, CA) is also mounted on the vehicle. On April 19, sea bottom surveys were located in the Gulf of Riga (Fig. 9). A total of 6822 CTD samples were conducted from 5- to 32-m depth while surveying an area of around 1 km^2 searching for OOIs. A CTD cast was done from the *NR/V Alliance* with a CTD SeaBird 911 in the neighborhood of the surveyed area to provide a validation data set. Fig. 10 summarizes the collected data set. Notice that the CTD validation cast is out of the convex hull spanned by AUV observations. Thus, estimating thermal values at this validation location corresponds to an extrapolation instead of interpolation process. No meaningful temperatures were recorded when the vehicle surfaced. It has been hypothesized that this could be the result of hydrodynamic interference (flow) along the hull that prevented water through flow at the CTD intake. Thus,

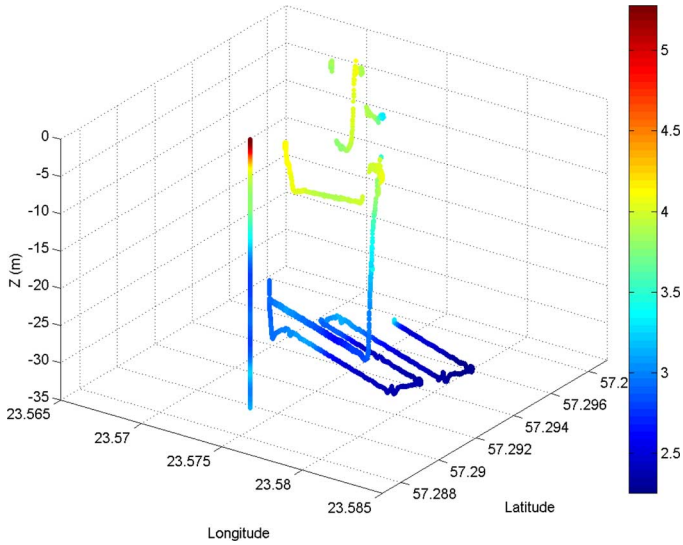

Fig. 10. Temperature data gathered by the Muscle AUV and CTD cast done for validation (straight vertical line). Colorbar units: degrees Celsius.

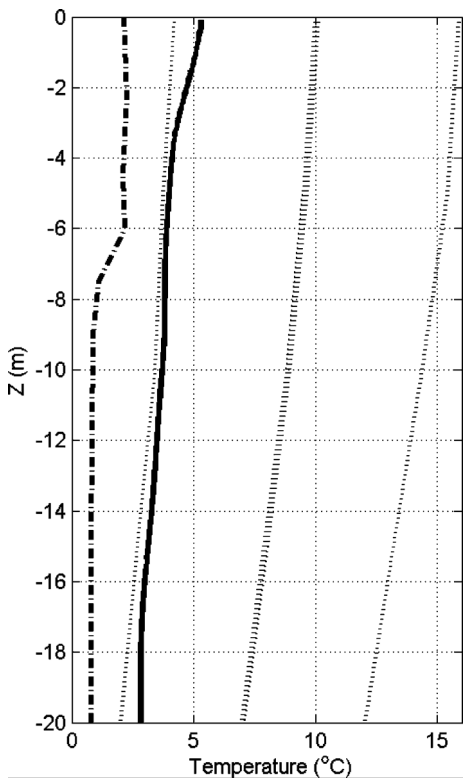

Fig. 11. CTD validation cast (solid line), climatologic profile (thick dotted line), and area delimited by the standard deviation (thin dotted lines) [32] and CTD cast done on April 6, 2009, in a nearby location [31].

information about the vertical structure of the water column is only used from the downcast profile of the vehicle. *In situ* measurements were complemented with an AVHRR multichannel sea surface temperature (MCSST) image of 1.1–km resolution from the same day (Fig. 9).

Fig. 11 compares the CTD validation cast with a climatologic profile obtained from CTD profiles regularly done during 1973–1995 in a station located 30 km northward from the sampling area [32]. The figure also includes a CTD profile done a

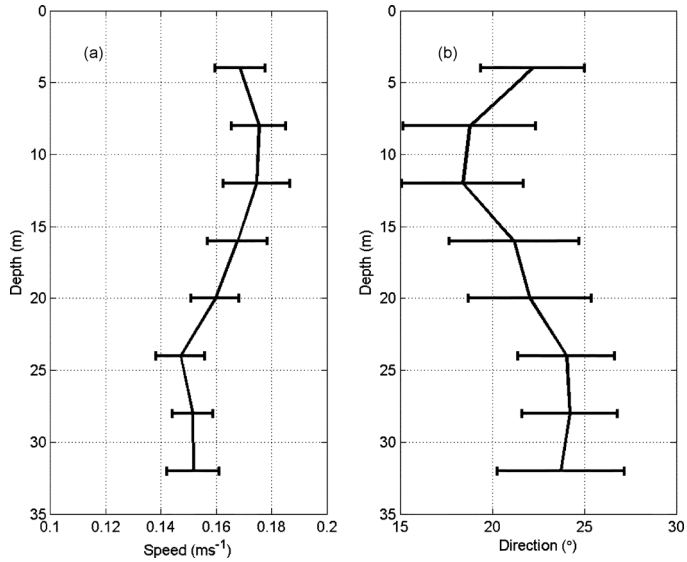

Fig. 12. (a) Current speed and (b) direction measured by the shipborne ADCP during the sampling period.

year later, April 6, 2009, 15 km westward of the area of interest [31]. Different issues can be highlighted from Fig. 11. First, significant interannual valiability exists in the thermal conditions of the region. This is explained by the relevance of air masses to force local thermal stratification, the thermal structure of the water column being very sensitive to atmospheric conditions. These atmospheric conditions are dominated by short-term variations due to passing cyclones with a few days' time scale, with the addition of occasional blocking events, which typically lead to longer calm and warm periods in late spring and summer. Second, climatology does not seem representative of the temperature structure found in the water column during this period of the year. CTD casts measured during April 2008 and 2009 are near-outliers and ourliers, respectively, of the statistical model provided by climatology. This could result from the monitoring strategy followed in the Guld of Riga during 1973–1995 [32]: springtime conditions were normally recorded in May; summertime, in August; autumn, in October. Data coverage of other months was rather random. Winter conditions were recorded quite seldom because of the frequent ice coverage. Thus, climatology is expected to be biased towards thermal conditions characteristic of warm periods of the year.

Atmospheric forcing is the main source of short-term variability in the central part of the Gulf of Riga. Light breeze conditions (1.6–3.4 m/s) dominated this area from April 15 to April 19, resulting in a weak current field in the water column. Fig. 12(a) and (b) displays the intensity and direction of the current measured during the experiment with the shipborne WH-300 acoustic Doppler current profiler (ADCP) installed in the *NRV Alliance*. The background current field was northward with a speed of 0.16 ms^{-1}. This is an order of magnitude slower than the speed developed by the sampling platform. On the other hand, the spectrum of the AVHRR-MCSST imagery is peaked at spatial scales of 10 km. This scale agrees with the characteristic internal Rossby radius in the region (8 km). Thus, a local advective time scale of around 5.5×10^4 s (15 h) is

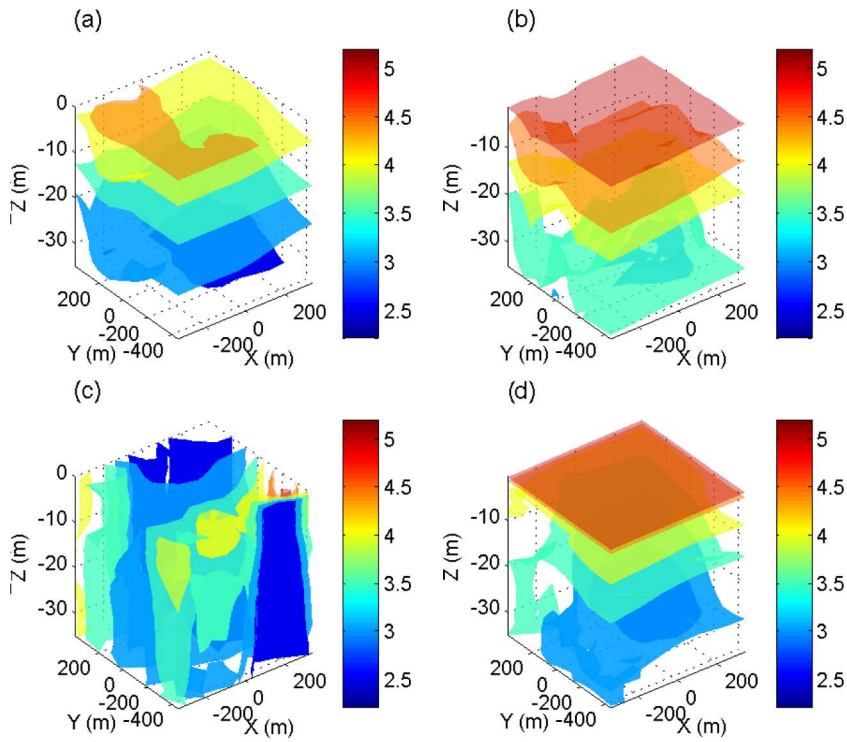

Fig. 13. Three-dimensional temperature reconstructions obtained from (a) the membrane model without satellite data, (b) the membrane model with satellite data, (c) the thin plate model without satellite data, and (d) the thin plate model with satellite data. Colorbar units: degrees Celsius.

expected. Unimodal seiches can induce significant variability at the center of the Gulf of Riga due to its semienclosed geometry. They are characterized by periods of 12 240 s (3.4 h) in this region. These characteristic time scales of the environmental processes occurring at the location of interest are significantly longer than the sampling time (1900 s), suggesting near-synoptic conditions during the sampling period.

Similar to the previous case, the domain was tessellated from the surface to a depth of 35 m with prismatic elements of 2.3-m height and triangular faces of approximately 150-m edges. This generated a grid of 1020 prismatic elements (68 elements per layer and a total of 15 layers) and 3140 nodes. This was the maximum resolution allowed in a dual core PC at 2.66 GHz and 2 GB of RAM. A computing time of 1587.9 s was required to run this numerical setup. Fig. 13(a)–(d) displays the reconstruction of the isothermals of 5 °C, 4.5 °C, 4 °C, 3.5 °C, 3 °C, and 2.5 °C obtained with the membrane and thin plate models without and with satellite information. A horizontally stratified field is obtained from the membrane model without satellite information [Fig. 13(a)]. The resulting surface field is 1 °C cooler than the real one. Fig. 13(b) shows the results obtained when satellite data are incorporated into the membrane model. Surface layers are now warmer, and a linear decrease with depth is observed. Notice the warm layer found at the bottom of the domain. Fig. 13(c) reveals that the thin plate model without satellite information results in a rather unstructured thermal field. The vertical cast is not able to constrain the vertical structure of the water column alone. Instead, bottom temperatures are extrapolated up to the surface. The reconstructed field changes drastically when the satellite information is integrated into the thin plate model [Fig. 13(d)]. An abrupt variation of the thermal field is observed in the most superficial layers. A thermal doming is found at the intermediate and deeper layers. This doming is an extrapolation of the temperature variability observed by the Muscle AUV with coolest temperatures located at the most distant corner of the domain.

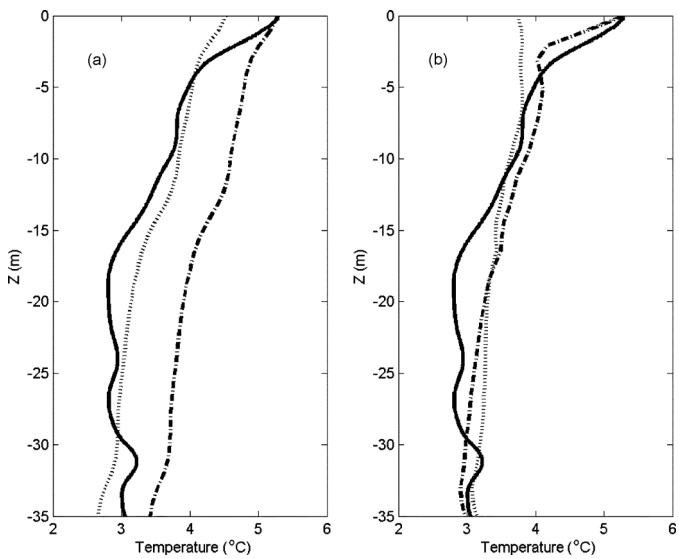

Fig. 14. (a) Comparison of the validation profile (solid line) with the profiles estimated from the membrane model without (dotted line) and with (dashed–dotted line) satellite data. (b) The same as (a) but for the thin plate model.

Fig. 14(a) and (b) provides further analysis of the results. Specifically, it compares the vertical profile of the reconstructed field with the CTD data, at the location where the CTD cast

was done. Concerning the membrane model, Fig. 14(a) shows a nearly constant gradient of the reconstructed temperature profile with depth. Incorporation of satellite information introduces an offset in the linear dependence of the temperature with depth but does not modify the rate of variability [Fig. 14(b)]. Fig. 14(c) confirms the behavior previously observed for the temperature field resulting from the thin plate model without satellite information. The profile extends the temperature measured at the bottom layer almost up to the surface. A substantial change is found when satellite data are considered [Fig. 14(d)]. The estimated profile shows a strong temperature gradient in the first 5 m of the water column that closely resembles the real profile. The decreasing rate is smaller below 5-m depth. The model overestimates the temperature at the middle layers and matches the deepest observations.

A more quantitative measure of the performance of the estimation models is provided by the so-called normalized explained variance

$$R^2 = 1 - \frac{\sum_{i=1}^{Np} \left(\hat{T}(z_i) - T(z_i)\right)^2}{\sum_{i=1}^{Np} \left(T(z_i) - \bar{T}\right)^2}$$

here $\hat{T}(z_i)$ and $T(z_i)$ are the estimated and observed temperatures at depths $\{z_i\}_{i=1}^{Np}$, N_p is the number of points used to describe the profile, and $\bar{T}$ is the vertically averaged temperature in the observed profile. R^2 is a dimensionless coefficient that compares the explained variance with the total variance of the data. It is commonly used as a metric to quantify the performance of prediction and estimation models, involving a direct comparison between observations and corresponding estimations. Values of R^2 close to one indicate good performance in the estimation, while values equal or less than zero are indicative of a poor estimation. R^2 is 0.79 for the membrane model without satellite data, -0.71 for the membrane model with satellite data, 0.47 for the thin plate model, and 0.81 for the thin plate model including satellite information. Results confirm the previous qualitative assessment of model performances, with estimations from the thin plate model with satellite information being the closest to the observed profile. Notice the poor performance obtained from the membrane model when satellite information is considered. This fact results from the strong thermal gradient found at the surface layer that invalidates the hypothesis of negligible gradients assumed in the membrane model. The model is imposed to fit surface temperatures that substantially differ from the thermal conditions beneath the surface. A positive offset in the thermal structure of the water column results in fit model estimations to imposed boundary conditions.

V. Discussion and Conclusion

This paper has investigated a mathematical framework to fuse information gathered by remote sensors and AUVs to produce a volumetric estimation of the observed field. Different factors have been considered. First, it has been assumed that the AUV does not perform a mission specially designed to obtain environmental data. Instead, it is considered as an AUV "of opportunity," i.e., an AUV that systematically collects environmental data regardless of its primary missions. This is most likely to occur when employing AUVs in military operations.

A second problem when dealing with environmental data collected by AUVs concerns the enormous size of the generated data set. Roughly speaking, AUVs can provide a sample of an oceanographic field every meter. Thus, data sets of hundreds of thousands of samples can be generated easily during a mission. Data analysis methods traditionally employed in oceanography are limited to fairly moderate data sets. Alternative approaches must then be considered. Summarizing, the scenario considered here is that of providing a 3-D view of an oceanographic field using remote sensing and data densely gathered on a general 1-D AUV trajectory.

The theoretical framework chosen to solve this problem is the MAP probability. This procedure relies on merging the prior knowledge with the likelihood estimation using a Bayes rule. Smoothness of the field was assumed *a priori*. This generally involves constraints on the first or second derivatives of the field. These are called membrane and thin plate models, respectively. Other assumptions on derivatives of higher order could be established. However, they were discarded in this work for computational reasons. The MAP problem has been solved using a variational approach. Variational techniques provide an elegant way to incorporate information about the boundaries, i.e., to introduce in the estimation information obtained by remote sensors.

Finite elements were employed to solve the variational problem. A finite element described by a prismatic geometry involving 15 nodes per element was considered. This element is sufficiently accurate to compute first- and second-order field derivatives. An interesting computational aspect of this technique when applied to this estimation problem is that the computational complexity depends on the number of nodes of the mesh and not on the size of the data set. Thus, the approach is able to process a huge amount of data. This is of particular relevance in the problem considered here due to the big data set generated by AUVs. Computational limitations due to mesh size are more tractable with unstructured mesh methods such as finite elements. For a constant number of nodes, mesh resolution could be higher in the neighborhoods of the AUV trajectory than in the remaining regions. The impact of multiresolution on near- and far-field estimations remains an open issue and will be considered in a future work.

The methodology has been first applied in an academic experiment. Volumetric estimations using membrane and thin plate models with and without satellite information were done from data collected on a virtual AUV trajectory in the simulated environment. Several conclusions can be drawn from these numerical tests. Both model approaches provide reasonable volumetric estimations of the oceanographic field even when the AUV follows trajectories quite unfavorable for environmental sampling. Incorporation of satellite information improves estimations done with the thin plate model but degrades the results from the membrane model. In the latter, surface information strongly affects the estimated temperature field at the deepest layers. The prior energy

$$F(\psi) = \int\int_V \int |\nabla\psi|^2 dxdydz$$

considered in membrane models takes the minimum value of zero only if the field is spatially constant. Thus, it is assumed that the spatial variability in the AUV data is partially originated by random deviations from a background constant value. Dirichlet boundary conditions at surface fix the value of the background field biasing estimations beneath sea surface. Fields with constant spatial gradients minimize the prior energy

$$F(\psi) = \int_V \int \int \left|\nabla^2 \psi\right|^2 dxdydz$$

considered in thin plate models. Thus, the observed variability is hypothesized as deviations from a background field with a constant spatial gradient. The impact of surface boundary conditions is lower at deep layers because more degrees of freedom are involved in the estimation. In both cases, the coarse resolution of the remotely sensed data can degrade the performance of the method in those areas with significant small-scale variability. There, estimations can substantially differ from point measurements. Only finer samplings of these regions with *in situ* or remote sensors could correct this deficiency.

Estimation procedures were also validated in a field experiment carried out by the Muscle AUV in the Gulf of Riga on April 19, 2008. CTD data were collected by the vehicle while performing a mine countermeasure mission. Unlike in the simulated experiment, only a vertical cast of the water column was available due to unexpected blocking of the flow through the CTD pipe when the vehicle moved towards surface. A profile was estimated with the approaches considered in a location where a CTD cast was previously done for validation purposes.

Measurements were assumed synoptic and so, no time dependence was considered in the analysis. Synopticity is determined by the characteristic time scales of the environmental processes occurring at a given location, ranging from hours in some energetic coastal environments up to a week in the open ocean. It limits the time scale of applicability of any estimation technique that does not include time as variable. Estimation procedures can be extended to deal with nonsynoptic measurements, but their computational complexity and information requirements about the physical processes in the region are substantially increased. In this study, the synoptic time scale is expected to be longer than the time required for the AUV to complete the sampling. Weak wind and calm conditions dominated the region before and during the experiment and thus, their induced variability was expected negligible. The estimated advection time scale and natural seiche periods are longer than the time employed by the AUV to sample the area. These issues reinforce the hypothesis that the reported experiment was done under synoptic conditions.

Membrane models with and without satellite data generate estimations with a linear dependence of the temperature with depth. Incorporation of satellite information introduces a temperature offset in the whole water column to fit the surface constraints. Results shown strong impact that vertical undersampling of the water column has on the estimations of the thin plate model when satellite information is not considered. Bottom temperatures are almost constantly extrapolated to the surface, generating an unrealistic thermal field in the domain. Incorporation of satellite information substantially corrects the deficiencies found in the thin plate model estimations when remote sensing data are not considered. The estimated profile captures part of the features observed in the measured profile, showing a strong thermal gradient in the first 5 m of the water column, continuing with a linear relationship of the temperature field with depth and matching the observed temperatures at the deepest layers.

Concluding, a guideline of applicability for the spline models results from this study. In general, spline models are suitable to estimate volumetric conditions from AUVs of opportunity when no *a priori* knowledge of the variability in the region is available and the sampling is synoptic and dense but unequally distributed. Membrane models are more suitable than thin plate models when vertical AUV casts are sparse and no satellite information is available. Including satellite data in membrane models is not recommended if the AUV trajectory is beneath the mixed layer. Comparison between SST and CTD data collected by the AUV can provide an initial estimation of the vertical thermal gradient, and determine the convenience of using a membrane model. Thin plate models are more appropriate when the AUV performs several vertical excursions in the volume or when satellite information is available. Incorporating satellite information to a thin plate model has shown to be the best approach to infer volumetric variability from AUVs of opportunity.

Acknowledgment

The work of the officers and crew of the *NR/V Alliance*, the scientist in charge of the *Colossus-2* trial, and NURC personnel is greatly appreciated. The author would like to thank Dr. E. Coiras for comments to the original manuscript. Finally, the author also acknowledges comments from anonymous reviewers.

References

[1] D. M. Barker, W. Huang, Y.-R. Guo, A. J. Bourgeois, and Q. N. Xiao, "A three-dimensional variational data assimilation system for MM5: Implementation and initial results," *Monthly Weather Rev.*, vol. 132, no. 4, pp. 897–914, 2004.

[2] S. L. Barnes, "A technique for maximizing details in numerical weather map analysis," *J. Appl. Meteor.*, vol. 3, no. 4, pp. 396–409, 1964.

[3] M. Berman, "Automated smoothing of image and other regularly spaced data," *IEEE Trans. Pattern Anal. Mach. Intell.*, vol. 16, no. 5, pp. 460–468, May 1994.

[4] M. W. Berry and K. S. Minser, "Algorithm 798: High dimensional interpolation using the modified Shepard method," *ACM Trans. Math. Softw.*, vol. 25, no. 3, pp. 353–366, 1999.

[5] E. Bohnsack, "Continuous field approximation of experimentally given data by finite elements," *Comput. Structures*, vol. 63, no. 6, pp. 1195–1204, 1997.

[6] P. Brasseur, "A variational inverse method for the reconstruction of general circulation fields in the northern Bering Sea," *J. Geophys. Res.*, vol. 96, no. C3, pp. 4891–4907, 1991.

[7] P. Brasseur and J. A. Haus, "Application of a 3-D variational inverse model to the analysis of ecohydrodynamic data in the Northern Bering and Southern Chucki Seas," *J. Mar. Syst.*, vol. 1, no. 4, pp. 383–401, 1991.

[8] A. Caiti, A. Munafò, and R. Viviani, "Cooperating autonomous underwater vehicles to estimate ocean environmental parameters," presented at the IARP Int. Workshop Underwater Robot., Genova, Italy, Nov. 7–9, 2005.

[9] J.-P. Chiles and P. Delfiner, *Geostatistics: Modeling Spatial Uncertainty*. New York: Wiley, 1999, pp. 720–720.

[10] C. Courtier, J. Derber, R. Errico, J. F. Louis, and T. Vukicevic, "Important literature on the use of adjoint, variational methods and the Kalman filter in meteorology," *Tellus*, vol. 45A, no. 5, pp. 342–357, 1993.

[11] T. Curtin, J. Bellingham, J. Catipovic, and D. Webb, "Autonomous oceanographic sampling networks," *Oceanography*, vol. 6, no. 3, pp. 86–94, 1993.

[12] R. Daley, *Atmospheric Data Analysis*. New York: Cambridge Univ. Press, 1999, pp. 457–457.
[13] G. Dhatt and G. Touzot, *The Finite Element Displayed*. New York: Wiley, 1984, pp. 509–509.
[14] S. Dobrici and N. Pinardi, "An oceanographic three-dimensional variational data assimilation scheme," *Ocean Model.*, vol. 22, no. 3–4, pp. 89–105, 2008.
[15] Z. Feng and R. E. Rowlands, "Continuous full-field representation and differentiation of three-dimensional experimental vector data," *Comput. Structures*, vol. 26, no. 6, pp. 979–990, 1987.
[16] R. L. Hardy, "Multiquadratic equations of topography and other irregular surfaces," *J. Geophys. Res.*, vol. 76, no. 8, pp. 1905–1976, 1971.
[17] C. Harris, "The omniscient eye: Satellite imagery, "battlespace awareness" and the structures of the imperial gaze," *Surveillance Soc.*, vol. 4, no. 1–2, pp. 101–122, 2006.
[18] X.-Y. Huang, Q. Xiao, D. M. Barker, X. Zhang, J. Michalakes, W. Huang, T. Henderson, J. Bray, Y. Chen, Z. Ma, J. Dudhia, Y. Guo, X. Zhang, D.-J. Won, H.-C. Lin, and Y.-H. Kuo, "Four-dimensional variational data assimilation for WRF: Formulation and preliminary results," *Monthly Weather Rev.*, vol. 137, no. 1, pp. 299–314, 2009.
[19] H. Inoue, "A least-squares smooth fitting for irregularly spaced data: Finite element approach using the B-cubic spline basis," *Geophysics*, vol. 51, no. 11, pp. 2051–2066, 1986.
[20] J. Jagiello, "Stable numerical solution of the adsorption integral equation using splines," *Langmuir*, vol. 10, no. 8, pp. 2778–2785, 1994.
[21] J. Jordan, "Remus AUV plays key role in Iraq War," *Underwater Magazine*, 2003 [Online]. Available: http://www.best-maritime-crewing.info/catalogue_companies_list/company_source_48531_14.html
[22] A. Katz, *Principles of Statistical Mechanics-The Information Theory Approach*. San Francisco, CA: W. H. Freeman, 1967, pp. 188–188.
[23] F. Le Dimet and O. Talagrand, "Variational algorithms for analysis and assimilation of meteorological observations: Theoretic aspects," *Tellus*, vol. 38A, no. 2, pp. 97–110, 1986.
[24] S. Levedev, A. Sirota, D. Medvedev, S. Khlebnikova, S. Vignudelli, H. M. Snaith, P. Cipollini, F. Venuti, F. Lyard, J. Bouffard, J. F. Cretaux, F. Birol, L. Roblou, A. Kostianoy, A. Ginzburg, N. Sheremet, E. Kuzmina, R. Mamedov, K. Ismatova, A. Alyev, and B Mustafayev, "Exploiting satellite altimetry in coastal ocean through the ALTICORE project," *Rus. J. Earth. Sci.*, vol. 10, 2008, ES1002.
[25] S. Z. Li, *Markov Random Field Modeling in Computer Vision*. New-York: Springer-Verlag, 1995, pp. 264–264.
[26] Z. Li, Y. Chao, J. McWilliams, and K. Ide, "A three dimensional variational data assimilation scheme for the regional ocean modeling system: Implementation and basic experiments," *J. Geophys. Res.*, vol. 113, 2008, DOI: 10.1029/2006JC004042, C05002.
[27] B. Luong, J. Blum, and J. Verron, "A variational method for the resolution of a data assimilation problem in oceanography," *Inverse Problems*, vol. 14, no. 4, pp. 979–997, 1998.
[28] D. Maes and D. Behringer, "Using satellite-derived sea level and temperature profiles for determining the salinity variability: A new approach," *J. Geophys. Res.*, vol. 105, no. C4, pp. 8537–8547, 2000.
[29] P. C. McIntosh, "Oceanographic data interpolation: Objective analysis and splines," *J. Geophys. Res.*, vol. 95, no. C8, pp. 13529–13541, 1990.
[30] A. Pascual and D. Gomis, "Use of surface data to estimate geostrophic transport," *J. Atmos. Ocean. Technol.*, vol. 20, no. 6, pp. 912–926, 2003.
[31] H. Pettersson, R/V Aranda Cruise Report 04/2009, Finnish Environment Institute, Helsinki, Finland, 2009, pp. 1–14.
[32] U. Raudsepp, "Interannual and seasonal temperature variations in the Gulf of Riga and corresponding saline water inflow from the Baltic proper," *Nordic Hydrology*, vol. 32, no. 2, pp. 135–160, 2001.
[33] J. A. Rice, *Mathematical Statistics and Data Analysis*. Belmont, CA: Duxbury Press, 1995, pp. 650–650.
[34] A. R. Robinson, J. Sellschopp, W. G. Leslie, A. Alvarez, G. Baldasserini, P. J. Haley, P. F. J. Lermusiaux, C. J. Lozano, E. Nacini, R. Onken, R. Stoner, and P. Zanasca, "Forecasting synoptic transients in the Eastern Ligurian Sea," in *Rapid Environmental Assessment, SACLANTCEN Conference Proceedings Series CP-46*, E. Bovio, R. Tyce, and H. Schmidt, Eds., SACLANTCEN, La Spezia, Italy, 2003.
[35] K. Shaw and N. Brown, "Unmanned vehicles enter the underwater battlespace," Jane's Navy Int., 2002 [Online]. Available: http://search.janes.com/
[36] R. Scott, "Future undersea battlespace: Unmanned, undersea," *Jane's Defense Weekly*, vol. 37, no. 24, pp. 28–34, 2002.
[37] D. Shepard, "A two dimensional interpolation function for irregularly spaced data," in *Proc. 23rd ACM Nat. Conf.*, New York, 1968, pp. 517–524.
[38] L. M. Stein, *Interpolation of Spatial Data*. New York: Springer-Verlag, 1999, pp. 246–246.
[39] A. Tarantola, *Inverse Problem Theory*. Philadelphia, PA: SIAM, 2005, pp. 342–342.
[40] A. M. Thompson, "Estimating the sun's rotation from solar oscillations by regularisation," *Astron. Astrophys.*, vol. 265, no. 1, pp. 289–295, 1992.
[41] O. C. Zienkiewicz and R. L. Taylor, *The Finite Element Method. Basic Formulation and Linear Problems*. Maidenhead, U.K.: McGraw-Hill, 1995, pp. 648–648.
[42] G. Wahba, *Spline Models for Observational Data*. Philadelphia, PA: SIAM, 1990, pp. 165–165.
[43] G. Wahba, D. R. Johnson, F. Gao, and J. Gong, "Adaptive tuning of numerical weather prediction models: Randomized GCV in three-and four-dimensional data assimilation," *Monthly Weather Rev.*, vol. 123, no. 11, pp. 3358–3369, 1995.

Alberto Alvarez received the M.S. degree in physics from the University of Santiago de Compostela, Santiago de Compostela, Spain, in 1991, the Ph.D. degree from the Physics Department, University of Balearic Island, Balearic Island, Spain, in 1995, the second Ph.D. degree in underwater robotics from the Department of Electrical Engineering, University of Pisa, Pisa, Italy, in 2004, and the D.E.A. in ocean engineering and marine technology from the Polytechnic University of Madrid, Madrid, Spain, in 2007.

Professionally, he was an Assistant Professor with the University of Balearic Island from 1995 to 1997. He received a postdoctoral position with the Physics Department, National Central University, Jhongli City, Taiwan, from 1997 to 1999, to work in underwater acoustics. In 1999, he joined the Department of Rapid Environmental Assessment, SACLANT Undersea Research Centre, La Spezia, Italy, as a Scientist. Since 2002, he has been a Scientist in the Spanish National Council Research (CSIC). In 2008, he received a special leave from CSIC to join the Department of Systems and Technology, NATO Undersea Research Centre (former SACLANT Undersea Research Centre).

Document Data Sheet

Security Classification		Project No.
Document Serial No.	**Date of Issue**	**Total Pages**
NURC-PR-2012-003	April 2012	13 pp.

Author(s)

Alvarez, A.

Title

Volumetric reconstruction of oceanographic fields estimated from remote sensing and in situ observations from autonomous underwater vehicles of opportunity.

Abstract

A main challenge of military oceanography (MILOC) is to assess the oceanographic conditions of denied/high-risk marine regions. Monitoring technologies are limited to those that can provide access to these regions. Remote sensing and autonomous underwater vehicles (AUVs) can support MILOC requirements. Unfortunately, the environmental information gathered by these technologies is not complete: remote sensing provides information about some surface conditions and water-column integrated variables, whereas operational priorities often constrain AUVs use during real crisis situations to missions with higher priority than environmental assessment. Under this scenario, data fusion techniques to maximize the information of the collected data are essential. This paper attempts to reconstruct thermal fields fusing data gathered by remote sensing platforms and AUVs performing missions not specifically designed for environmental data collection. The technique estimates the state that maximizes the posterior probability subjected to some smoothing constraints. A variational methodology allows remote sensing information to serve as boundary constraints. The approach uses 3-D finite elements to solve the maximization problem. The procedure investigated has been tested with different smoothing constraints in a simulated environment and in a real field experiment conducted by the Muscle AUV in the Gulf of Riga (Baltic Sea) on April 19, 2008. Results highlight the relevance of incorporating the surface information provided by remote sensors into the estimation.

Keywords

Autonomous underwater vehicles (AUVs), finite elements, oceanographic sampling.

Issuing Organization

NURC
Viale San Bartolomeo 400, 19126 La Spezia, Italy

[From N. America:
NURC
(New York) APO AE 09613-5000]

Tel: +39 0187 527 361
Fax:+39 0187 527 700

E-mail: library@nurc.nato.int